Int J Earth Sci (Geol Rundsch) (2017) 106:1–17
DOI 10.1007/s00531-015-1290-z

ORIGINAL PAPER

Structural analysis of hanging wall and footwall blocks within the Río Guanajibo fold-and-thrust belt in Southwest Puerto Rico

Daniel A. Laó-Dávila[1] · **Pablo A. Llerandi-Román**[2,3]

Received: 1 June 2015 / Accepted: 19 December 2015 / Published online: 30 December 2015

Abstract The Río Guanajibo fold-and-thrust belt (RGFT), composed of Cretaceous serpentinite and volcano-sedimentary rocks, represents the deformation front of a contractional event in SW Puerto Rico during the Paleogene. Previous studies inferred structural and stratigraphic relationships from poorly exposed outcrops. New road cuts exposed the Yauco (YF) and El Rayo Formations (ERF) providing insights on the deformation of the hanging wall and footwall. We described the nature and orientation of faults and folds and analyzed the kinematic indicators to characterize the deformation. The YF occurs in the hanging wall and shows a sequence of folded, medium-bedded mudstone and thinly bedded shale and sandstone. Major folds strike NW–SE and are gentle with steeply inclined axial planes and sub-horizontal fold axes. Minor folds are open with moderately inclined axial planes and gently to moderately inclined SE-plunging fold axes. NW–SE striking reverse and thrust faults cut layers and show movement to the SW. Steep left-lateral faults strike NW–SE and NE–SW, and smaller right-lateral strike-slip faults strike NNE–SSW. At the footwall, the ERF consists of bioclastic limestone and polymictic orthoconglomerates and paraconglomerates. Reverse and strike-slip faults cut along lithological contacts. Results suggest that the hanging wall and footwall accommodated strain along preexisting weaknesses, which are dependent on lithology and sedimentary structures. The kinematic analysis suggests that shortening in the NE–SW direction was partitioned between folding and interlayer shortening, accommodated by flexural slip, and reverse and left-lateral faults that resulted from contraction. The RGFT represents the Paleogene back arc deformation of a bivergent thrust system.

Keywords Thrust faults · Kinematic analysis · Caribbean · Foreland · Island arc · Bivergent

✉ Daniel A. Laó-Dávila
daniel.lao_davila@okstate.edu

[1] Boone Pickens School of Geology, Oklahoma State University, 105 Noble Research Center, Stillwater, OK 74078-3031, USA

[2] Geology Department, Grand Valley State University, 118 Padnos Hall of Science, One Campus Drive, Allendale, MI 49401, USA

[3] Departamento de Ciencias Físicas, Facultad de Estudios Generales, Universidad de Puerto Rico, Río Piedras, PR 00931, USA

Introduction

Fold-and-thrust belts are major crustal deformational structures that accommodate strain in convergent plate boundaries (e.g., Boyer and Elliott 1982). In island arcs, fold-and-thrust belts form in accretionary prisms above the subduction zone (e.g., Davis et al. 1983). However, some island arcs also show back arc thrusts and folds with vergence opposite to the one in the fore arc, thus defining a bivergent thrust system (e.g., Willett et al. 1993; Naylor and Sinclair 2008; ten Brink et al. 2009). Modern examples of bivergent thrust systems occur in the Eastern Sunda Arc (Silver et al. 1983), Banda Arc (Snyder et al. 1996), Costa Rica (Plafker and Ward 1992; Suárez et al. 1995), Vanuatu (Lagabrielle et al. 2003), and Puerto Rico and Hispaniola (ten Brink et al. 2009).

Fold-and-thrust belts in Puerto Rico and Hispaniola formed within the transpressional Caribbean–North American plate boundary zone (Fig. 1a). Today, the offshore Muertos Thrust system represents the retrowedge deformation south of the arc complex in Puerto Rico and eastern

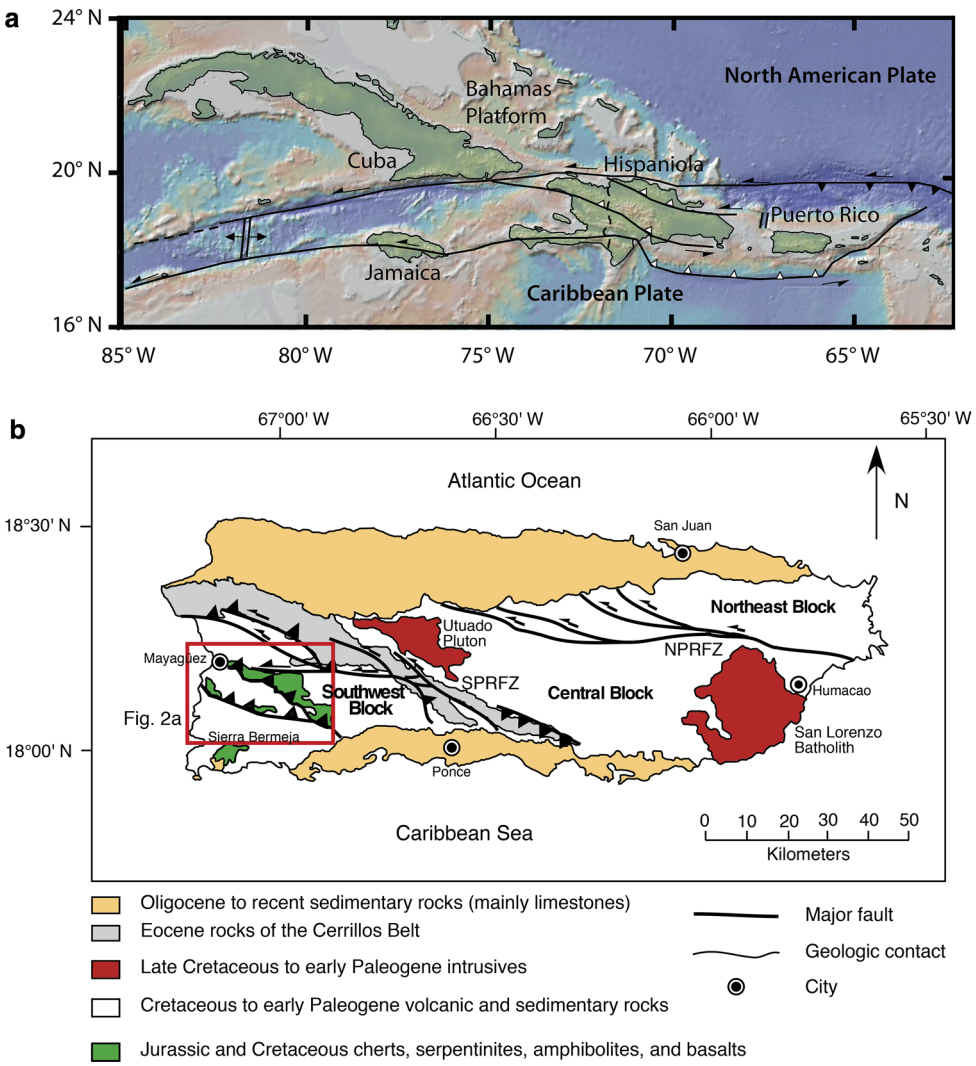

Fig. 1 **a** Map of the northeastern Caribbean showing major plate boundaries (modified from Wadge et al. 1984; GeoMapApp, http://www.geomapapp.org; Ryan et al. 2009; Laó-Dávila 2014), **b** geologic map of Puerto Rico (modified from Monroe 1980; Laó-Dávila 2014). *Red rectangle* shows area enlarged in Fig. 2a

Hispaniola (ten Brink et al. 2009). Moreover, older thrust systems are recognized in the back arcs of Puerto Rico and Hispaniola. For example, Paleogene and Neogene fold-and-thrust belts in the back arc of Hispaniola occur in the Sierra de Neiba, the Trois Rivieres–Peralta Terrane, and Río Ocoa Group (Witschard and Dolan 1990; Dolan et al. 1991; Mann et al. 1991; Heubeck and Mann 1991). In Puerto Rico, Paleogene fold-and-thrust belts include the Cerrillos belt, Monte del Estado belt, and the Río Guanajibo belt (Mattson 1960; Glover 1971; Erikson et al. 1990; Mann et al. 2005; Laó-Dávila et al. 2012; Laó-Dávila 2014).

The thrust systems in western Puerto Rico resulted from transpression along the Southern Puerto Rico Fault Zone and within the Southwest Block (Fig. 1b; Mattson 1960; Glover 1971; Laó-Dávila et al. 2012). In the Southwest Block (Fig. 2a), the NW–SE striking Monte del Estado and Río Guanajibo serpentinite belts were thrust to the SSW over folded Late Cretaceous volcano-sedimentary rocks, which were also thrust toward the SSW (Slowdowski 1956; Volckmann 1984; Laó-Dávila et al. 2012). Mattson (1960) suggested a deformation model for the southwest region in which NE–SW shortening formed large folds and thrust faults with strike-slip faults. Moreover, the prevalence of NW–SE striking thrust faults and fold axial planes, NW–SE and NE–SW striking strike-slip faults, E–W striking left-lateral faults, and oblique slip along thrust faults within the serpentinite indicate transpression in this region (Laó-Dávila and Anderson 2009; Laó-Dávila et al. 2012).

Although these studies have shown a regional model of deformation of fold-and-thrust belts in Southwest Puerto Rico, few details have been reported about folding mechanisms, kinematics, and strain accommodation within blocks of the fold-and-thrust belts. The lack of details is in part caused by the poorly exposed outcrops within the area.

To solve this problem, we studied three new road cuts that expose hanging wall and footwall blocks in the foreland of the Río Guanajibo belt (Fig. 2a). We conducted meso-scale structural analyses of rocks, folds, and fractures that define the geometry and kinematics of deformation within the blocks. The objectives of this study are to define

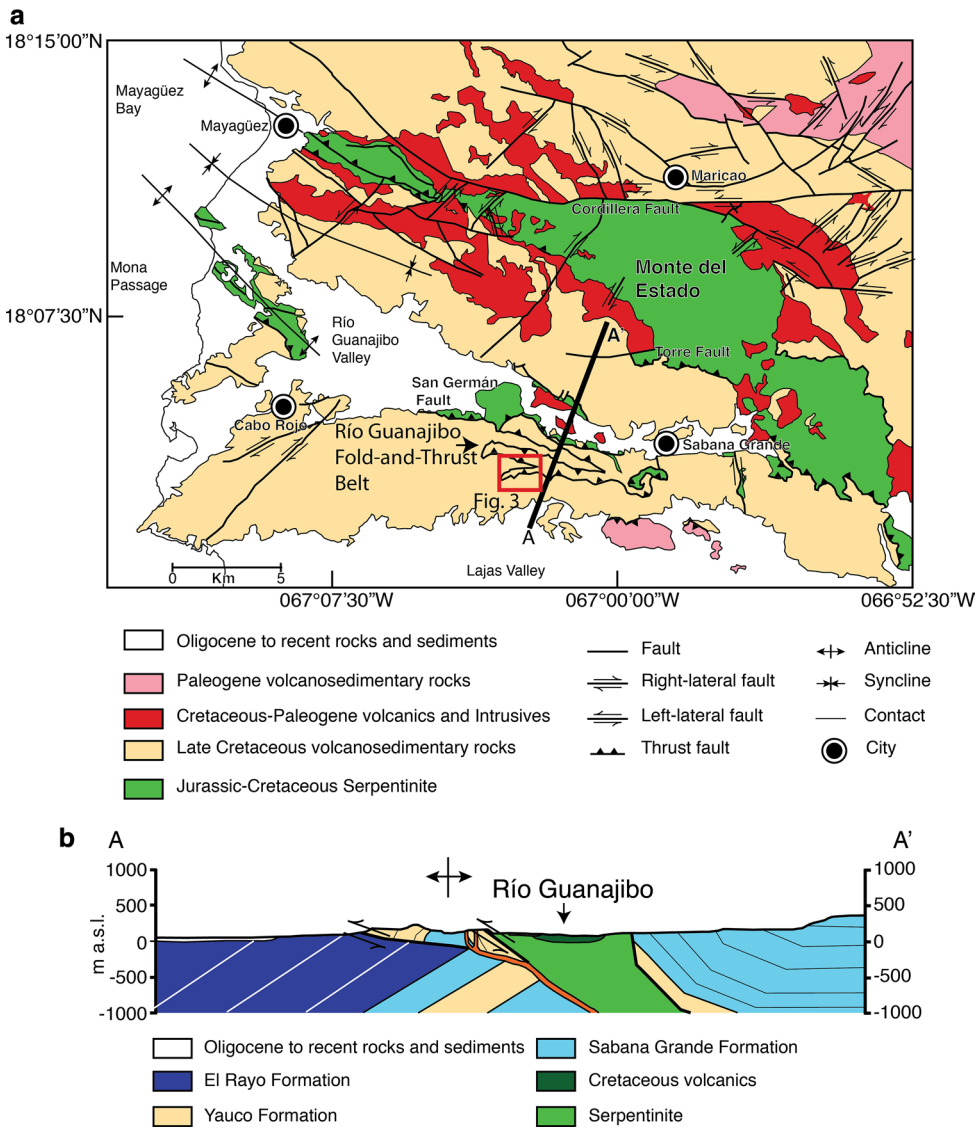

Fig. 2 **a** Geologic map of southwestern Puerto Rico (modified from Laó-Dávila 2014 and references therein). *Red rectangle* shows area enlarged in Fig. 3, **b** cross section of transect *A*–*A′* shown in **a** (modified from Laó-Dávila et al. 2012; Laó-Dávila 2014). No vertical exaggeration

the folding mechanism, the kinematics, and the accommodation of strain within the lithologically different hanging wall and footwall of the Río Guanajibo belt, a Paleogene back arc fold-and-thrust belt. These results will help improve models of strain of bivergent thrust systems and tectonic models of island arcs such as the systems in Hispaniola and the Muertos Trough.

Río Guanajibo fold-and-thrust belt

Structure

The Río Guanajibo fold-and-thrust belt (RGFT) extends from SW of Mayagüez on the west coast to the south of Sabana Grande, where it merges with the Monte del Estado serpentinite belt (Fig. 2a). The RGFT contains Cretaceous serpentinite and volcano-sedimentary rocks and represents the deformation front of a contractional event in SW Puerto Rico during the Paleogene. Evidence of this event is shown by structural relationships between the Río Guanajibo serpentinite, in the core of the RGFT, and adjacent volcano-sedimentary rocks. The Río Guanajibo serpentinite belt is thrust to the SW over the younger Yauco, Sabana Grande, and El Rayo Formations (Fig. 2b). The Yauco and Sabana Grande formations are in turn thrust over the tilted, and younger El Rayo Formation. These relationships occur in the foreland of the RGFT (Laó-Dávila et al. 2012). The San Germán Thrust Fault, between Cabo Rojo and Sabana Grande (Fig. 2a), is the principal fault above which serpentinite, Mariquita Chert, and Yauco Formation are thrust onto the Sabana Grande Formation (Volckmann 1984). Laó-Dávila et al. (2012) used crosscutting relationships to suggest that the age of

thrusting was in the Paleocene with reactivation in the late Eocene.

Formations

The rock units that form part of the RGFT are the Río Guanajibo serpentinite, the Sabana Grande Formation, the Yauco Formation, and the El Rayo Formation (Volckmann 1984; Laó-Dávila et al. 2012). The Río Guanajibo serpentinite occupies the core of the thrust belt and formed from harzburgite, dunite, and spinel lherzolite during Early Jurassic to Early Cretaceous epochs (Hess and Otalora 1964; Mattson 1964; Lewis et al. 2006; Laó-Dávila et al. 2012). The Sabana Grande Formation consists of massive volcanic and calcareous conglomerate and breccia, andesitic lava flows, sandstone, mudstone, and rare limestone (Slowdowski 1956; Mattson 1960; Volckmann 1984; Llerandi Román 2004). The Sabana Grande Formation is Campanian to early Maastrichtian in age based on fossil data and the interbedded relationship with the Yauco Formation (Curet 1981; Volckmann 1984; Llerandi Román 2004). Next, we describe in more detail the Yauco and El Rayo Formations as these units are the focus of this study.

The Yauco Formation consists of conglomerate and interbedded sandstone, siltstone, and mudstone. The composition of coarser-grained rocks ranges from reworked volcanogenic grains, especially granule to gravel-sized volcanic clasts in polymictic conglomerates, to calcareous sandstones. Finer-grained rocks are mainly calcareous, with minor carbonaceous mudstones and siliceous rocks that locally grade into hard, dark-gray to black chert (Mattson 1960; Volckmann 1984; Llerandi Román 2004). Calcareous mudstone, rich in planktonic foraminifera and radiolaria of Campanian to Maastrichtian age, indicate the age of the formation, which may be 500–2800 m thick (Slowdowski 1956; Mattson 1960; Pessagno 1960, 1962; McIntyre et al. 1970; Curet 1981).

The El Rayo Formation forms the core of a mountain range between the Río Guanajibo Valley and the northeastern boundary of the Lajas Valley to the south, from San Germán to the SE of Sabana Grande (Volckmann 1984; Martínez Colón 2003; Llerandi Román 2004). The formation consists of basaltic and andesitic flows, volcaniclastic and volcanogenic epiclastic conglomerates, and coarse-grained lithic sandstone interbedded with massive- to thin-bedded bioclastic limestone lenses and beds (Slowdowski 1956; Mattson 1960; Volckmann 1984; Santos 1999; Martínez Colón 2003; Llerandi Román 2004). These lenses grade from grain-supported lithic-rich limestone conglomerate to fossiliferous limestone with abundant foraminifera, gastropods, calcareous algae, and bivalves (oysters and rudists), with variable proportions of wackestone and packstone within a sequence. In addition, volcanic clasts locally occur within the limestone lenses. Limestone beds are steeply tilted and are more resistant to weathering than the volcanic and volcaniclastic rocks, forming conspicuous elongated hills along the exposure zone of the formation. The age of the El Rayo Formation, based on fossil assemblages, extends from latest Campanian into the early Maastrichtian (Volckmann 1984; Santos 1999; Mitchell et al. 2012).

Methods

Study site

The study site is located within the foreland of the RGFT (Figs. 2, 3). The construction of the new road PR-122 produced road cuts that expose in unprecedented detail the structures in this belt. Three stations where chosen for their excellent exposures along the road cuts between kilometer markers 1.1 and 1.8: two in the Yauco Formation (ST9W and ST9E; north hill), and one in the El Rayo Formation (ST11; south hill). The geologic map of the area shows the Yauco and Sabana Grande formations in the hanging wall and the El Rayo Formation in the footwall of the thrust system (Fig. 3).

Description of lithology and structures

At the three sites (Fig. 4), we described the lithology and nature of the structures of the hanging wall and footwall blocks using meso-scale observations in the field, and photographs and sketches in the laboratory. We also measured orientations of bedding, faults, folds, veins, and stylolites. In addition, we noted crosscutting relationships and type of deformation with the senses of shear along faults. The

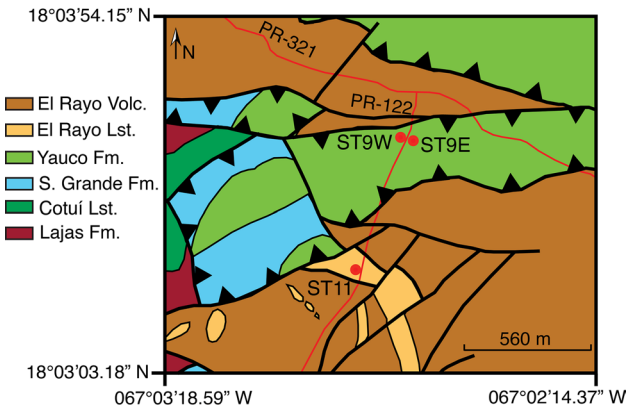

Fig. 3 Geologic map of the study area (modified from Volckmann 1984). *Red curves* are roads and *red circles* are the study sites

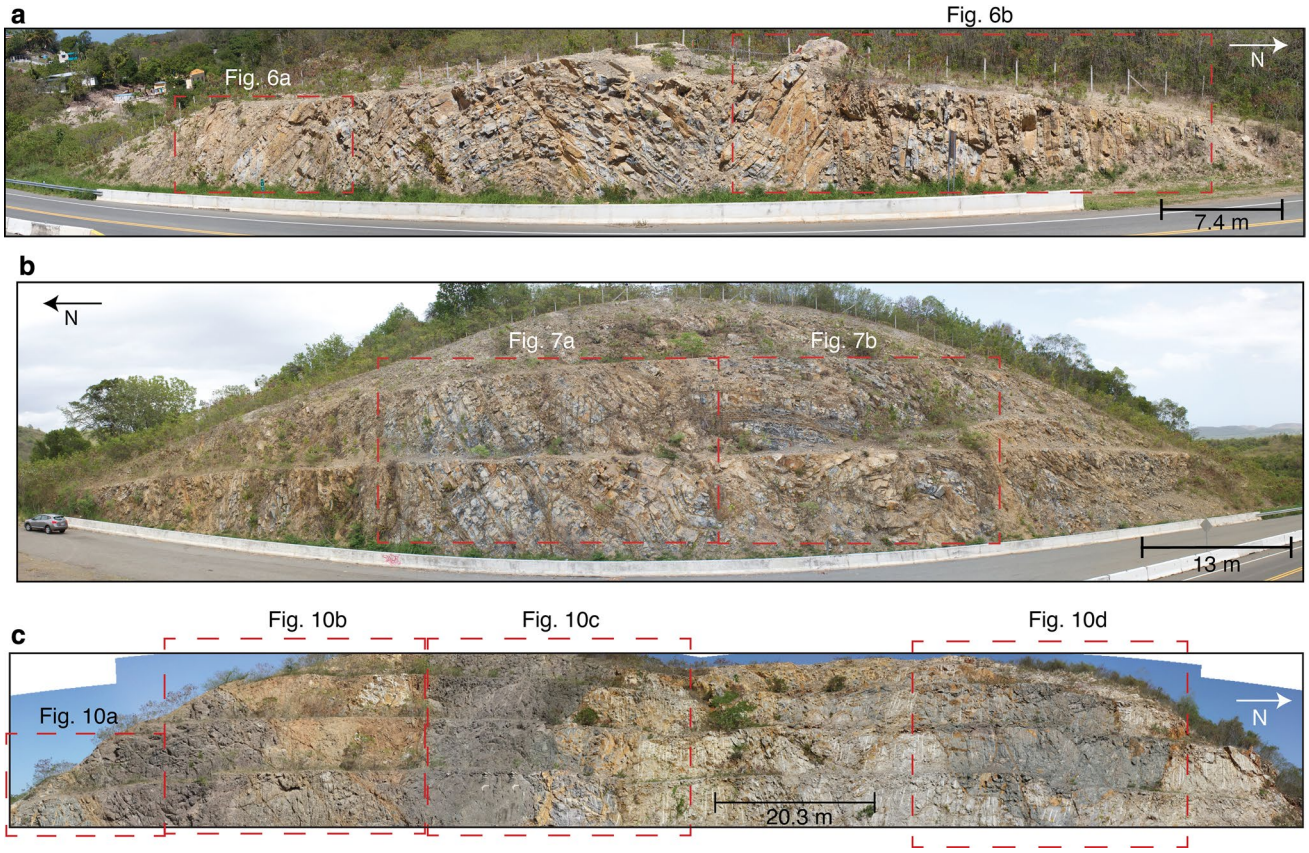

Fig. 4 Panoramas of road cuts in the Yauco and El Rayo Formations. **a** Site ST9W, **b** site ST9E, **c** site ST11. *Red dashed rectangles* show areas enlarged in Figs. 6, 7 and 10

descriptions and orientations were used to conduct a geometric analysis of deformation.

Kinematic analysis

We conducted a kinematic analysis using the orientations, slip directions, and sense of slip along faults. Sense of slip along faults was determined by offset of rock layers, drag folds, and steps in slickensided surfaces. Only faults that had slip directions and reliable senses of slip were used in this study. Fault-slip data were plotted on equal-area stereographic projections and analyzed for incremental strain principal directions. Shortening and extension (*P* and *T*) axes were calculated using the method from Marrett and Allmendinger (1990) and used in Laó-Dávila and Anderson (2009). Shortening and extension axes and tangent lineations were calculated using the Faultkin software (Marrett and Allmendinger 1990). Faults were grouped based on their type and orientation. The kinematic analysis assumes the following: (1) sampling is representative, (2) no post-faulting reorientation of the fault-slip directions, and (3) fault kinematics are scale-invariant (Marrett and Allmendinger 1990).

Results

The hanging wall

Lithology

The Yauco Formation in the hanging wall (ST9W and ST9E) shows a sequence of folded, medium-bedded mudstone and thinly bedded shale, with scarce thickly bedded, medium to fine-grained sandstone layers. Thin (2–4 cm thick) and foliated shale layers occur between mudstone layers. Mudstone layer thickness ranges from 9 to 150 cm, with an average of 20 cm. The mudstone contains rare pyrite aggregates up to 3 cm in length. Medium- to fine-grained sandstone layers show normal grading (coarsening upwards).

Structures

Bedding of the Yauco Formation in ST9W and ST9E strike NW–SE with poles that define a NE–SW striking girdle (Fig. 5a). Folds have sub-horizontal to moderately

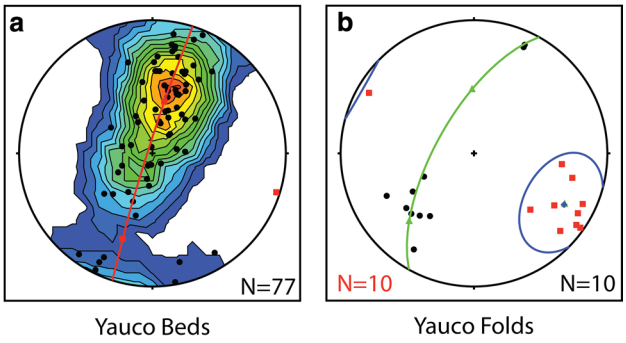

Fig. 5 Lower hemisphere stereographic projections of bedding and folds in the Yauco Formation (sites ST9W and ST9E). **a** Kamb contour of poles to bedding. NNE–SSW striking girdle suggests similar shortening direction, **b** *black-filled circles* are poles to axial planes, *red squares* are fold axes, *blue ellipse* is 95 % confidence area, and *green great circle* is cylindrical best-fit for poles of axial planes

inclined SE-plunging fold axes and SE–NW striking and moderately to steeply inclined fold axial planes with vergence toward the SW (Fig. 5b). A gentle syncline-anticline pair with amplitude of 2.9 m and wavelength longer than 16 m defines the structure of ST9W (Fig. 4a). Drag folds occur next to faults throughout the hanging wall road cuts (Figs. 6, 7). Several open minor folds occur in ST9E (Figs. 5b, 8a).

Faults in ST9W and ST9E are thin discrete surfaces or wide tabular zones composed of fault breccia. The southern portion of ST9W shows SW-dipping strata cut by steep faults (Fig. 6a). A thrust fault underneath folded layers is cut by a steep normal fault composed of thick fault breccia (Fig. 6a). On the northern part of ST9W, sub-vertical strata are cut by thrust and reverse faults (Fig. 6b). On the southern part of ST9W, a steep zone with reverse and left-lateral faults cuts along the hinge of the anticline. Most reverse and thrust faults dip to the NE and suggest transport toward the SW (Fig. 6b). To the east, faults in north-central ST9E have reverse and left-lateral sense and cut across the SW-dipping layers and folded sequence (Figs. 7a, 8b). South-central ST9E contains strike-slip faults and fewer thrust faults than on the north-central part (Fig. 7b).

Slickensided fault surfaces contain striations and calcite steps that indicate the direction and the sense of movement along the faults (Fig. 8c). Some fault surfaces occur

Fig. 6 Photographs showing bedding (*white curves*) and fractures (*red curves*) in site ST9W. **a** Moderately dipping mudstone layers are cut by steep and shallow faults. Movement along faults folded the layers, **b** steeply dipping layers are cut by thrust and steep faults. *Insets* shows fault orientations in a lower hemisphere stereographic projection for each image

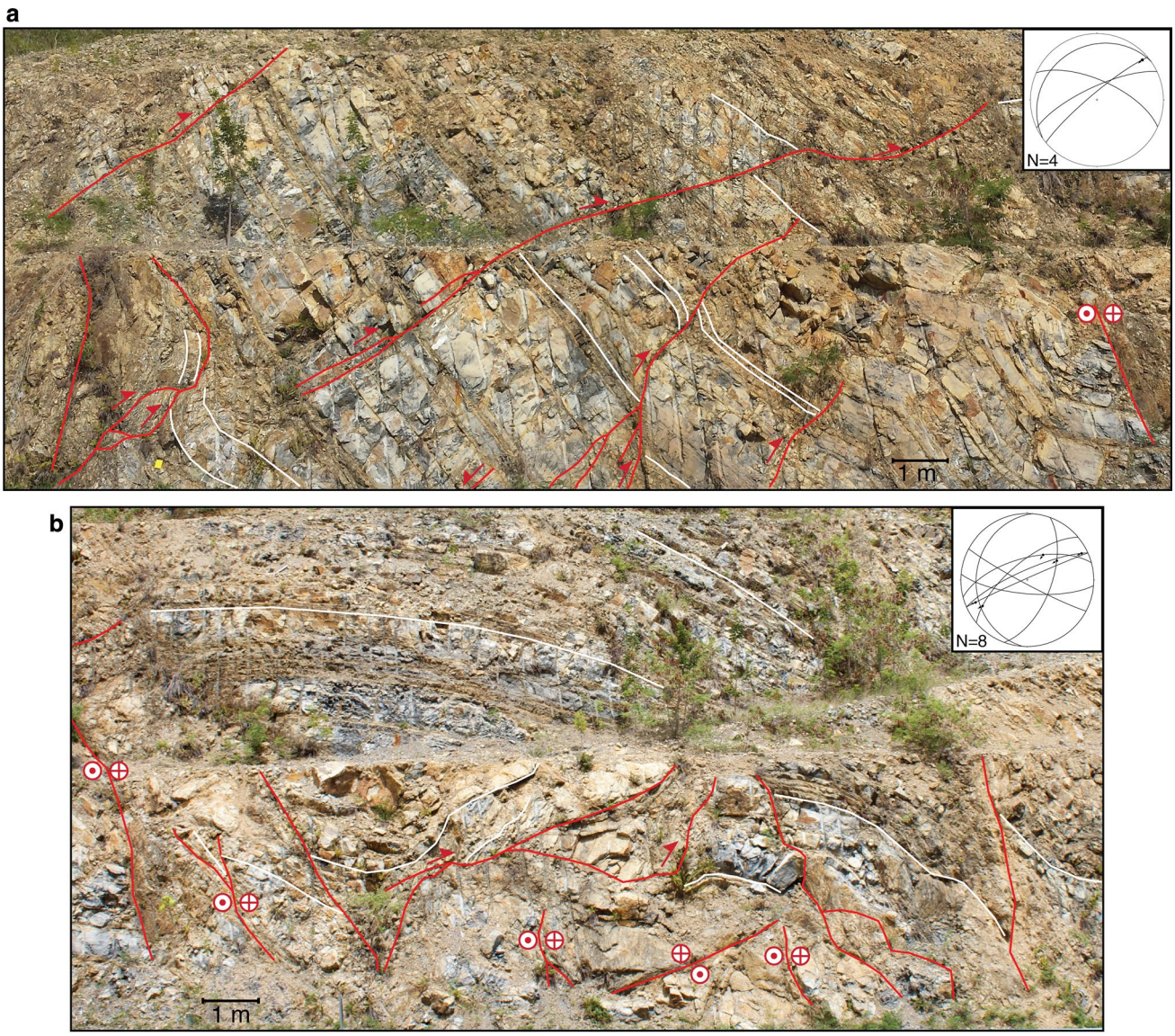

Fig. 7 Photographs showing bedding (*white curves*) and fractures (*red curves*) in site ST9E. **a** Layers are cut by reverse faults. *Drag folds* show sense of movement, **b** thrust and strike-slip faulting in the southern section of the road cut. *Insets* shows fault orientations in a lower hemisphere stereographic projection for each image

between rock layers and form a flat-ramp thrust geometry and duplex structures (Fig. 8d).

Fault orientation and striated plane data in ST9W and ST9E are shown in Fig. 9. The main group of faults consists of reverse and thrust faults. These faults strike NW–SE and have moderate- to low-angle surfaces, which mostly dip toward the NE (Fig. 9). Shale layers have S–C foliations that also suggest reverse faulting (Fig. 9). Left-lateral faults were the second most common group of faults. These faults strike ENE–WSW and WNW–ESE and dip steeply (Fig. 9). Right-lateral faults strike NNE–SSW and normal faults strike NE–SW (Fig. 9).

Crosscutting relationships show that the reverse faults cut the folded bedded sequence. In addition, strike-slip faults cut reverse faults in some places and in others are connected to the reverse faults. Thus, crosscutting relationships suggest that reverse and left-lateral faults are coeval. A large normal fault (Fig. 6a) is younger as it cuts the other faults and is composed of unconsolidated fault breccia. No crosscutting relationship could be established for the right-lateral faults.

The layers in ST9W and ST9E contain conspicuous white and brown-orange calcite veins (Fig. 8e, f). The brown-orange veins cut the white calcite veins and are interpreted as younger. Veins of both colors are described

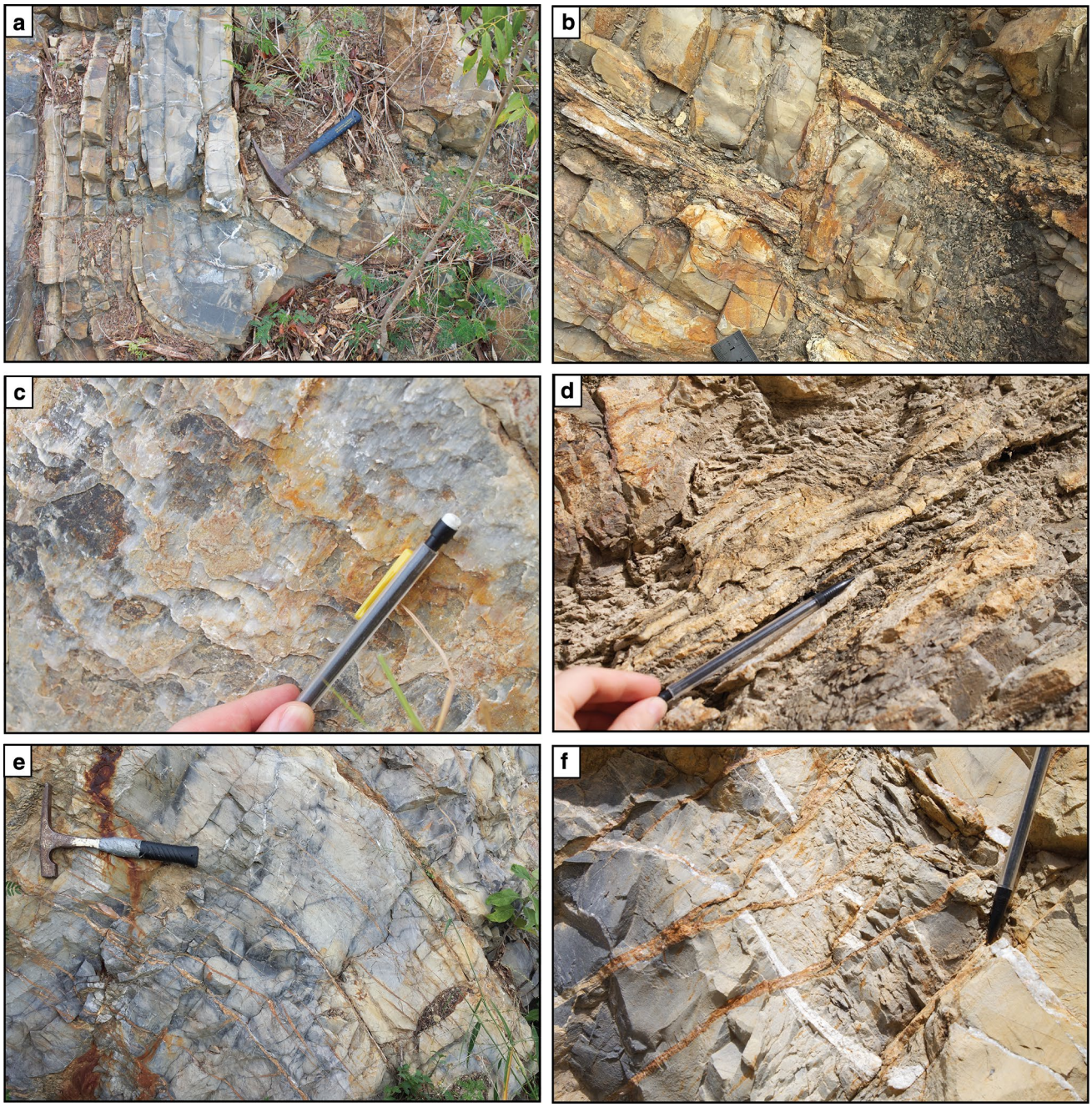

Fig. 8 Photographs of meso-scale structures within sites ST9W and ST9E. **a** Small fold in the mudstone. Hammer is 32 cm long, **b** steep reverse fault cutting and offsetting beds of the Yauco Formation, **c** steps and striations in slickenside plane at bedding contact. Pencil is 14.5 cm long, **d** thrust faults forming fault-bend folds at the contact of bedding planes, **e** layer-parallel calcite veins, **f** *Brown-orange* hybrid calcite veins cutting white calcite veins

as bed-parallel veins (Fig. 8e), veins at a high angle to bedding, hybrid veins (Fig. 8f), en échelon veins, and veins forming the matrix of breccia. Bedding-parallel veins are concentrated between layers and at fold hinges. Veins at high angle to bedding occur in the limbs, less in hinges of folds, and form conjugate pairs in places. Bedding-perpendicular joints show twist hackles and cut the veins, which suggests that they are younger than the veins.

Orientation data for veins in the Yauco Formation are shown in Fig. 9. Most veins are oriented perpendicular to the strike of bedding and strike NE–SW with moderate to steep dip. However, two groups of veins strike NW–SE

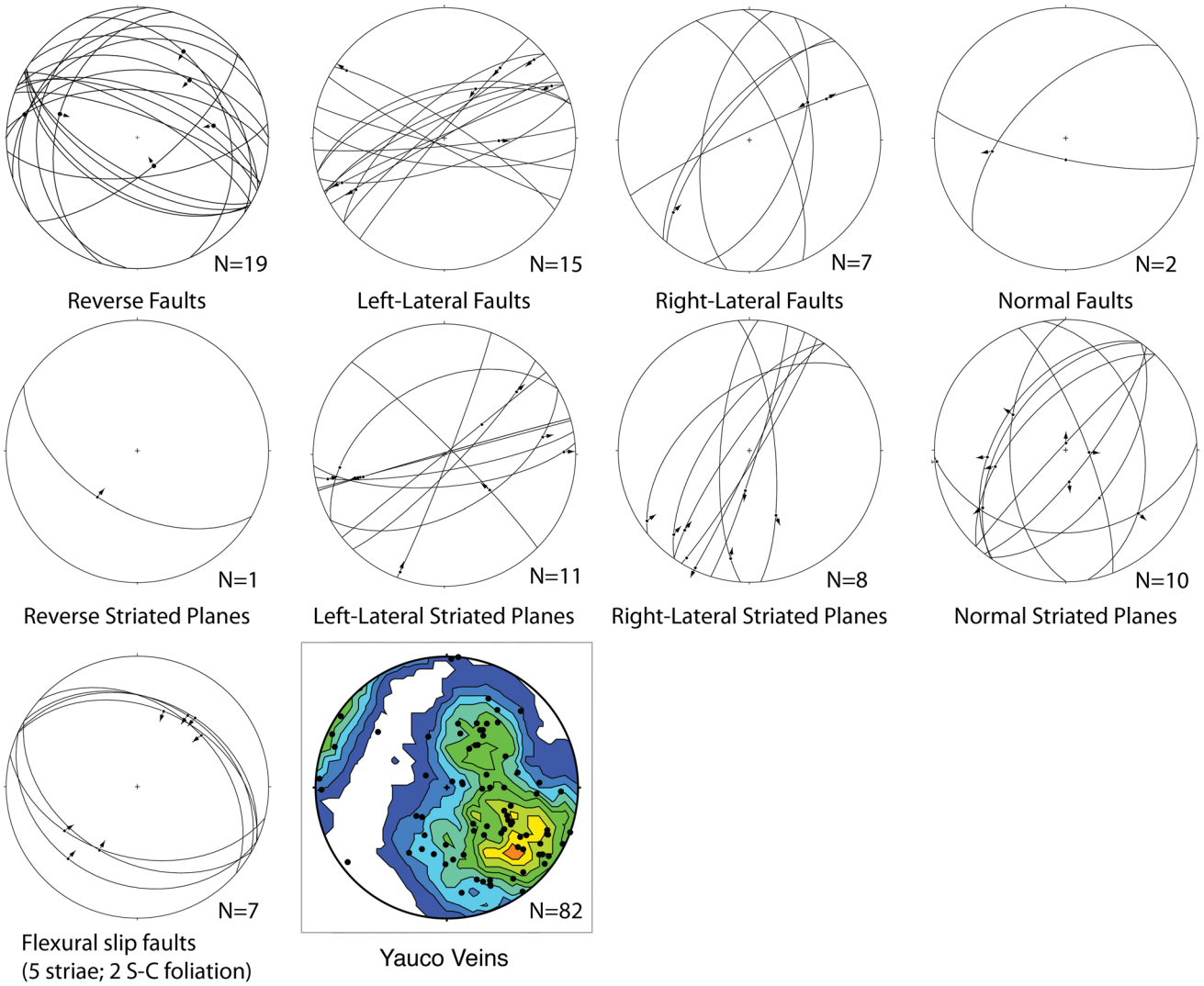

Fig. 9 Lower hemisphere stereographic projections of faults, striated planes, and veins. *Arrows* show direction of movement of the hanging walls of faults and shear planes. Faults interpreted as forming due to flexural slip are grouped together. Kamb contours show distribution of poles to veins within the Yauco Formation (sites ST9W and ST9E)

with moderate dip and opposite dip direction (Fig. 9). These veins occur at high angle to bedding and parallel to bedding.

The footwall

Lithology

At the footwall, the El Rayo Formation consists of rudist-bearing bioclastic limestone, lithic-rich limestone conglomerate, and volcanogenic polymictic orthoconglomerates and paraconglomerates (Fig. 10). At the southern end of the outcrop (Fig. 10a), two beds are exposed: (a) a massive bioclastic limestone (Fig. 11a), and (b) a matrix supported, lithic-rich limestone conglomerate (Fig. 11c). The massive bioclastic limestone consists of gray mudstone–wackestone with some localized packstone zones. It also contains well-preserved whole and fragmented fossils of *Parastroma* sp. and other unidentified species. This massive bioclastic limestone is in a transitional, possibly depositional, contact with the matrix supported, lithic-rich limestone conglomerate to the north (Fig. 10a).

The lithic-rich limestone conglomerate contains abundant (30–40 %) subangular–subrounded mafic-intermediate volcanic clasts, and fewer rudist fragments, mainly *Parastroma* sp. The matrix consists of wackestone–packstone with 10 % or more of 0.5–4 cm long subangular–subrounded bioclasts (including rudist shell fragments). Toward the south, subangular to subrounded volcanic clasts are 5–8 cm long, while toward the north, subangular to

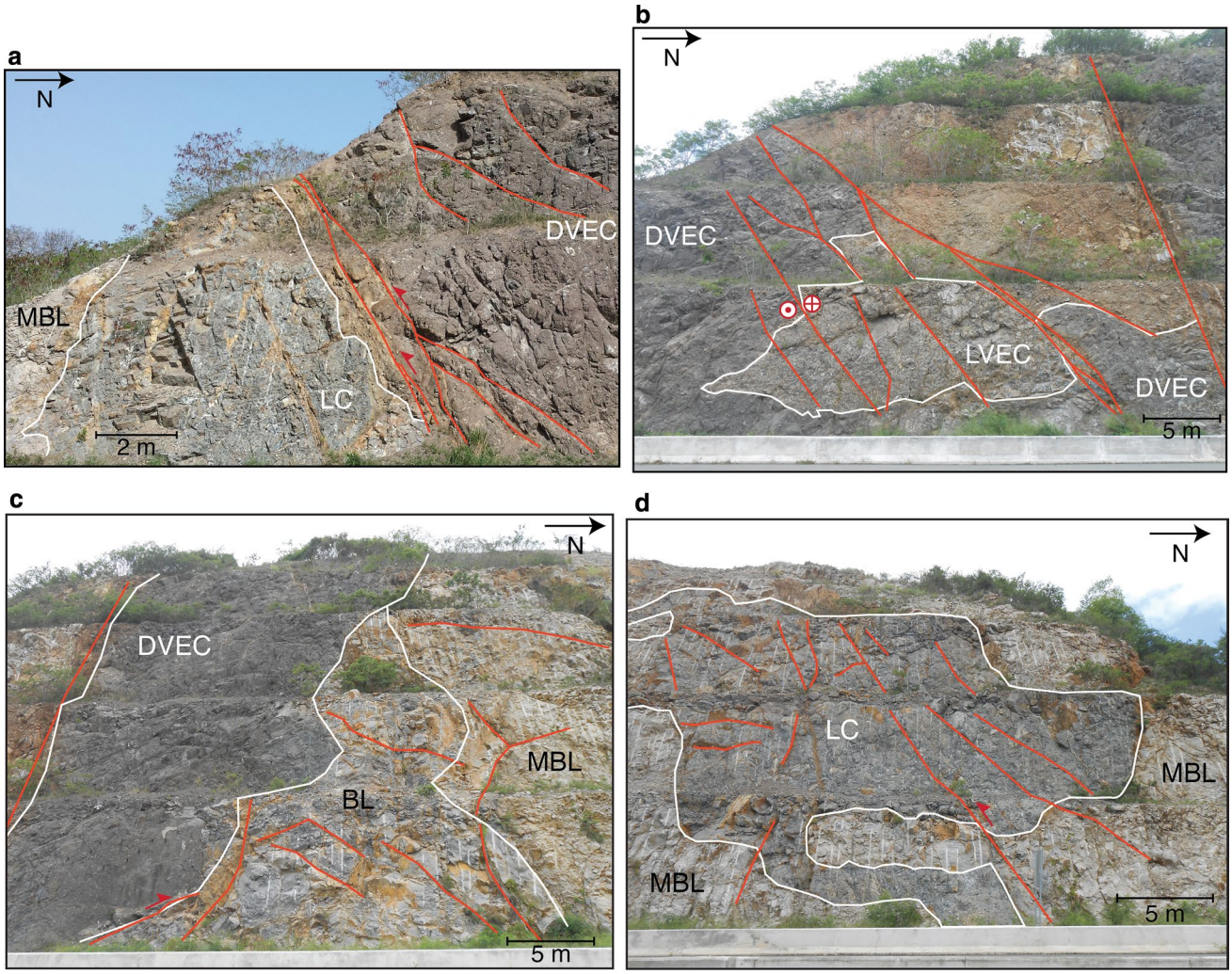

Fig. 10 Photographs showing contacts (*white curves*) and fractures (*red curves*) in site ST11. **a** Southern section showing massive bioclastic limestone (MBL), limestone conglomerate (LC), and dark volcaniclastic and epiclastic conglomerate (DVEC). The DVEC is thrust over the LC, **b** south-central section showing the light volcaniclastic and epiclastic conglomerate (LVEC) inside the DVEC and under the complex zone of faulted blocks, **c** northern half section showing the bioclastic limestone (BL) wedged between a DVEC and MBL, **d** northern section shows a large irregular mass of LC within the MBL

angular volcanic clasts are 6–20 cm long. On its north side, this unit is in fault contact with the dark volcanogenic and epiclastic conglomerate (Figs. 10a, 11d) that is part of the complex faulted region described below.

In the south-central section of the outcrop, there is a complex zone where several irregular faulted blocks of volcanogenic and epiclastic conglomerates occur (Fig. 10b). A light volcanogenic and epiclastic conglomerate block is located within a dark volcanogenic and epiclastic conglomerate. A highly weathered conglomerate with several subrounded to angular blocks of limestone 0.5–5 m long, in a gravel to sandy matrix lies above the volcanogenic and epiclastic conglomerates (Fig. 10b). To the north of these rock bodies, there is a gray, bioclastic limestone with a packstone–grainstone matrix, locally conglomeratic, with gravel-sized volcanic clasts (Fig. 10c).

A massive bioclastic limestone occupies the northern half of the outcrop and is in contact with an irregularly shaped lens of a lithic-rich limestone conglomerate (Figs. 10d, 11b) similar to the conglomerate in the southern end of the outcrop. This lens is composed of subrounded–subangular volcanic clasts 1–12 cm long (5–8 cm is the main size fraction) mixed with limestone clasts, including rudist bivalves and fragments of rudist shells (Fig. 11c). The conglomerate is predominantly clast-supported, although locally clasts are supported in a packstone–grainstone matrix. Volcanic clasts decrease their abundance toward the north. The contacts of this lens with the massive

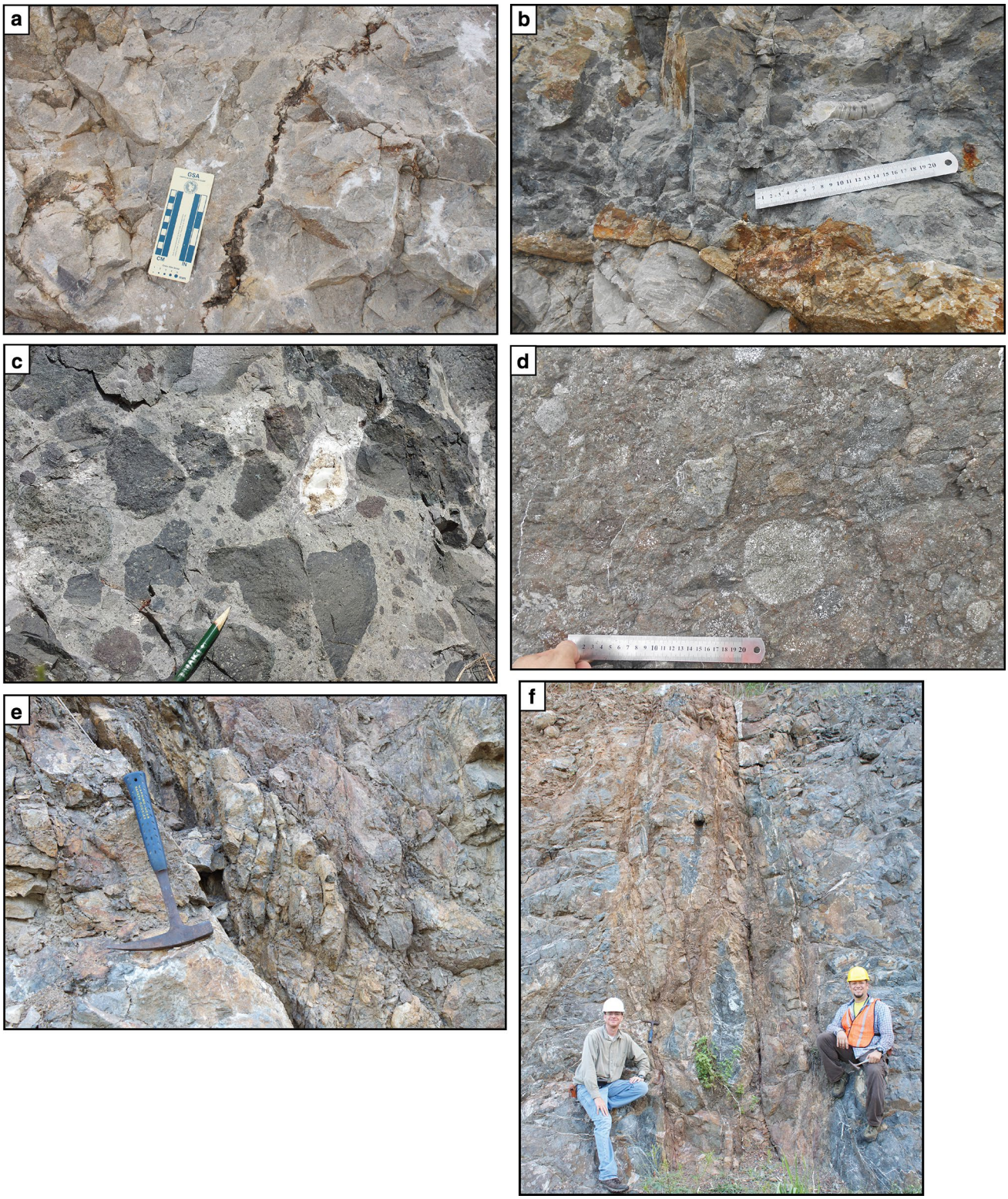

Fig. 11 Photographs of meso-scale structures within site ST11. **a** Stylolite within massive bioclastic limestone (MBL). Scale is 10 cm long, **b** contact between MBL and limestone conglomerate (LC), **c** details of the LC with rudist clast, **d** close-up photo of the dark volcaniclastic and epiclastic conglomerate (DVEC), **e** horses in duplex structure within reverse fault separating DVEC and LC. Hammer is 32 cm long, **f** sub-vertical fault cutting DVEC. Authors show scale in photograph

bioclastic limestone are mainly faulted or abrupt (Fig. 11b). However, the contacts are transitional in a few places.

The northern bioclastic limestone is light gray, massive, and locally stylolitic (Figs. 10d, 11a). It is a wackestone (locally packstone) with numerous fragments of rudist bivalves in the matrix, and also contains some gastropod fossils. Well-exposed, whole or slightly fractured specimens of *Parastroma* sp., 10–20 cm long, occur as clasts throughout the limestone and decrease in abundance toward the south.

Structures

The El Rayo Formation contains many fractures within the blocks and faults located along lithological contacts (Fig. 10). Within the conglomerates, fracturing occurred in the matrix and around clasts. Many non-systematic joints occur within the massive bioclastic limestone on the northern half of the outcrop. Faults are abundant in the contacts; however, few faults were observed cutting through the limestone. Throughout the outcrop, faults occur as thin to wide zones that are stained brown in places. Major fault zones contain fault breccia and thrust duplexes that indicate sense of movement (Fig. 11e, f). Four steeply to moderately inclined reverse faults strike E–W and three of those show transport toward the south (Figs. 10, 12). Most of the faults with large fault traces are reverse faults. Left-lateral, right-lateral, and normal faults strike NE–SW and have small fault traces (Fig. 12). However, most faults have unknown sense of slip as there were not many observed offsets or preserved striations with reliable sense of motion (Fig. 12).

Stylolites in the massive limestone are red, brown, orange, and black (Fig. 11a). They have amplitudes of 0.2–3 cm, wavelengths of 0.2–6 cm, and lengths >80 cm. Serrated surfaces in the stylolites are moderately to steeply dipping to the SW and SE (Fig. 12). However, few stylolites dip to the NE and NW.

Discussion

Geometric and kinematic analyses of the hanging wall

The structure in the hanging wall is that of a folded and faulted sequence of calcareous mudstone and sandstone layers. Poles to bedding form a girdle that suggests NE–SW shortening (Fig. 5a). Major and small folds have fold axes that trend SE and NW and axial planes that strike SE–NW and dip NE. Both of these structures suggest that folds formed from NE to SW shortening. Most reverse and thrust faults strike NW–SE and dip to the NE, which along with the SW vergence of the folds, as deduced from the dip of the axial planes, suggest that transport was to the SW. In addition, veins with a strike of NE–SW formed at a high angle to the bedding and are compatible with a SE–NW extension (Fig. 9). Thus, orientation data from beds, folds, reverse and thrust faults, and veins suggest NE–SW shortening.

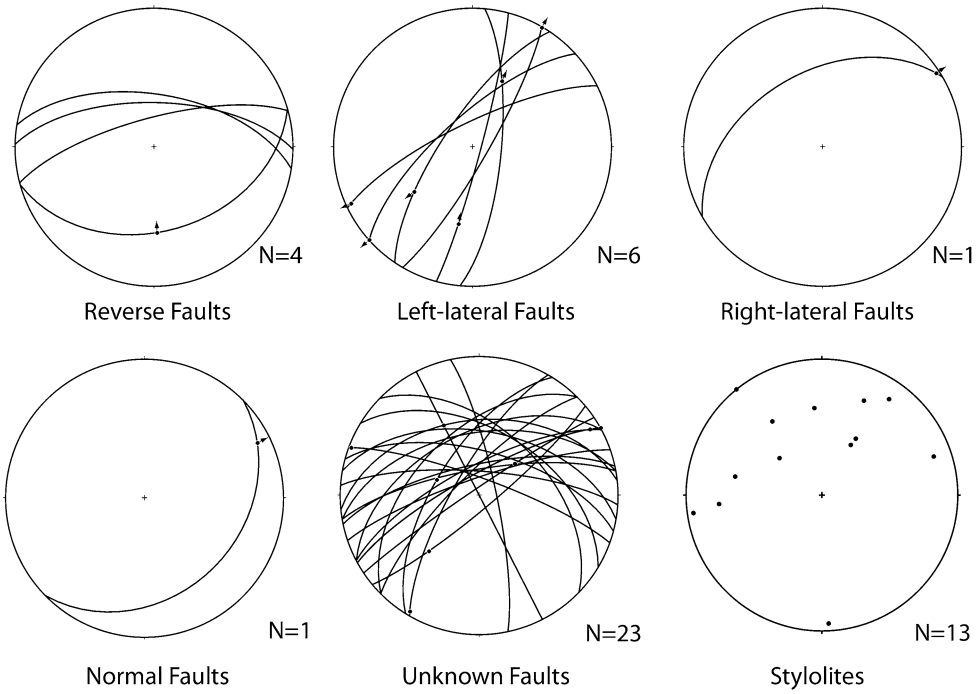

Fig. 12 Lower hemisphere stereographic projections of faults and poles to stylolites within the El Rayo Formation (site ST11). *Arrows* show direction of movement of the hanging walls

Kinematic analysis of faults and striated planes in the hanging wall shows the relationship between structures and how strain was accommodated. Reverse faults have shallow *P*-axes and steep *T*-axes as expected from contractional structures (Fig. 13). The shortening axes trend NE and SW and the extensional axes are steep, suggesting a NE–SW contractional regime, which agrees with the orientation data from the beds, folds, and veins. Left-lateral faults show NNE–SSW trending *P*-axes and WNW–ESE trending *T*-axes. These orientations suggest that the reverse and left-lateral faults may have formed during a similar NE–SW directed shortening event that was accommodated as pure shear strain. This is supported by the large coeval reverse and left-lateral structures observed in the outcrops.

In the case of the right-lateral faults, these show E–W trending *P*-axes and SSE–NNW trending *T*-axes (Fig. 13). We hypothesize that this E–W shortening is related to a later event in which steep structures were reactivated. This hypothesis is supported by the similarity of orientations of right-lateral faults with the left-lateral faults, and the fact that right-lateral faults consist of many striated planes or hybrid veins that are smaller than the reverse and left-lateral faults.

Normal faults show ESE–WNW *T*-axes with moderately plunging *P*-axes (Fig. 13). Slip directions in the fault planes show that most normal faults have a component of strike-slip and are better described as oblique faults. These slip directions, and the crosscutting relationship in which a

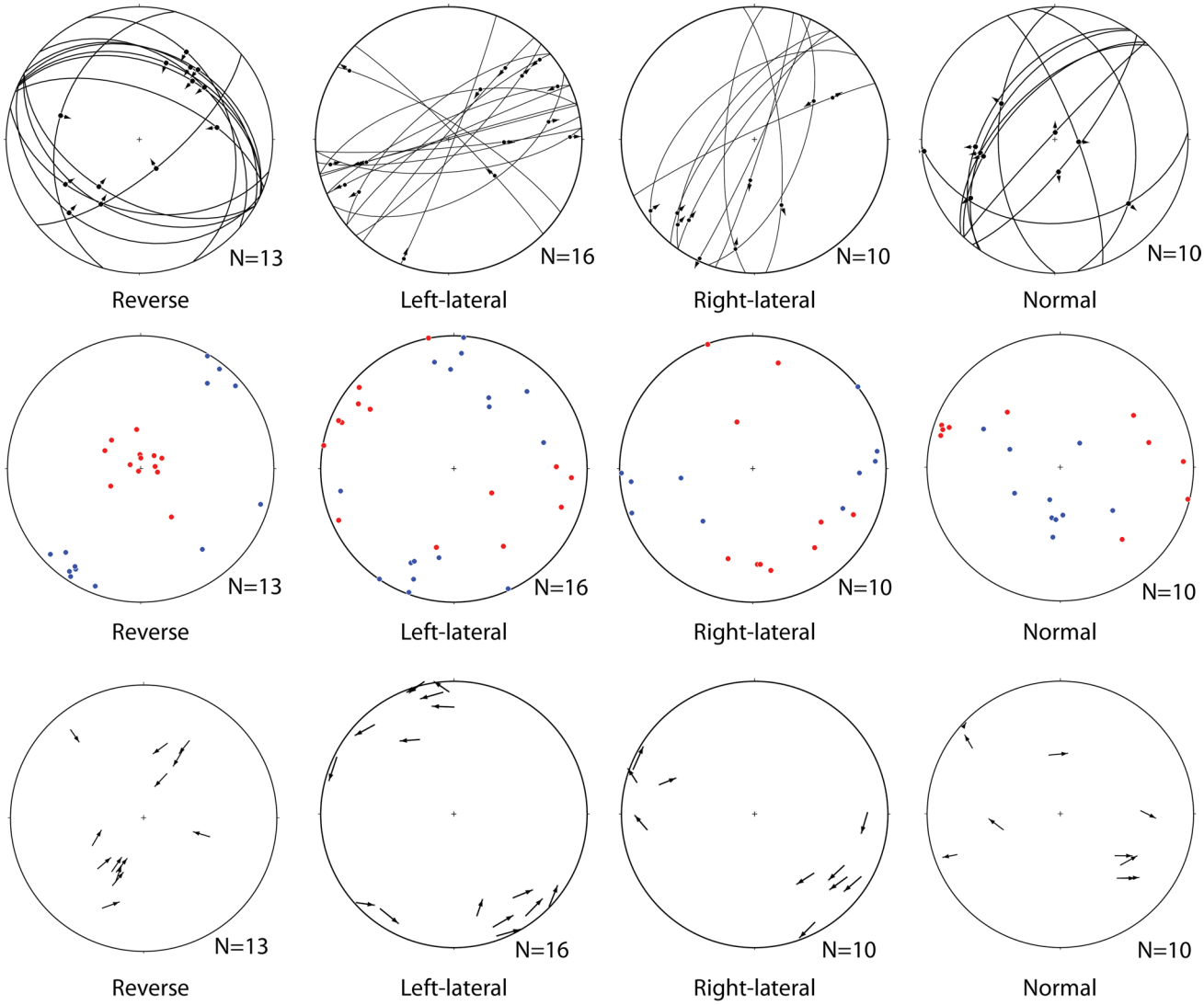

Fig. 13 Lower hemisphere stereographic projections showing kinematic data for faults in the Yauco Formation. *Top row* shows faults with known sense of slip and used in kinematic analysis. *Middle row* shows calculated *P*–*T* axes for faults. *Bottom row* shows tangent lineations for faults

steep normal fault cuts a thrust fault (Fig. 6a), suggest that normal faults are younger and may have formed during the reactivation of older structures.

Folding mechanism in the hanging wall

Structural data collected in this study suggest that major folds in the Yauco Formation (sites ST9W and ST9E) formed by a flexural slip mechanism (e.g., Tanner 1989, 1992; Fowler 1996). Boundaries between layers (especially shale layers) are filled with bed-parallel calcite veins with slip directions that indicate movement toward the hinge of the fold (Fig. 9) and are orthogonal to the trends of the fold axes (Fig. 5b). The occurrence of duplex structures within bed boundaries (Fig. 8d) and en échelon veins within the layers, with the same slip directions as the interlayer striations, support the flexural slip mechanism for the formation of these folds. The structures in these sites and the flexural slip mechanism suggest that strata were folded in the upper brittle crustal regime.

Geometric and kinematic analyses of the footwall

In contrast to the hanging wall, rocks on the footwall occur as faulted blocks with no clear orientations and no coherent sequence of stratification along the outcrop. However, in small contact areas between the north and south massive bioclastic limestone and the limestone conglomerates, there is evidence of transitional and abrupt contacts that could be gradational and thus, depositional. If this is the case, we interpret these contacts to occur within the faulted and discrete limestone–limestone conglomerate blocks, which in turn are faulted against the volcanogenic epiclastic conglomerates, and not an indication of lithostratigraphic units bounded by stratigraphic contacts throughout the outcrop. In general, the structure of the footwall is defined by a series of faulted blocks of rocks that originated in related volcanic and shallow marine environments, but with different lithological and structural characteristics, and not a series of stratigraphically bounded rocks.

For most of the faults in the footwall, we were not able to determine the sense of slip and direction of slip along the fault plane. However, the orientations of the fault planes without sense of slip and slip direction are similar to the reverse and left-lateral fault planes with known sense of slip and slip direction (Fig. 12). This similarity suggests that most of the faults with unknown sense of slip and slip direction may be reverse and left-lateral faults with a similar sense of slip and direction as the measured faults. Left-lateral faults have N–S trending *P*-axes and E–W trending *T*-axes, which suggest N–S shortening (Fig. 14). This shortening orientation is compatible with the orientations

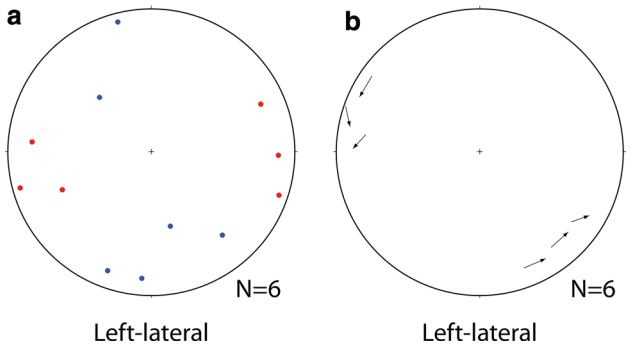

Fig. 14 Lower hemisphere stereographic projections showing kinematic data for left-lateral faults in the El Rayo Formation (Fig. 12). **a** Calculated *P*–*T* axes for faults, **b** tangent lineation for faults

of the reverse faults. The modest amount of evidence collected on the kinematics of faults in the footwall suggests that the reverse and left-lateral faults dominate the accommodation of strain and that a N–S shortening event produced the faults. ESE–WNW striking stylolites may have formed by the same shortening event, while the NNE–SSW striking stylolites may have formed by shortening during compaction normal to the surface (Fig. 12).

Strain localization

These results suggest that the hanging wall and footwall accommodated strain along preexisting surfaces of weakness, such as interlayer surfaces, contacts between units and blocks, and fractures. However, the different sedimentary structures (i.e., bedding vs. blocks) and composition of the hanging wall and footwall blocks were a controlling factor into the nature and location of the preexisting weaknesses and the localization of strain within the rocks. In the hanging wall, strain was accommodated by slip between medium-bedded and thinly bedded mudstone, formation of veins, and formation of folds by the flexural slip mechanism. Additional strain was principally localized along reverse, thrust, and left-lateral faults (e.g., Fig. 6b). Strain in the hanging wall, accommodated by flexural slip mechanism, may have been transferred from imbricate thrusts rooted in the detachment of the thrust sheet (Fig. 15). In the footwall, strain was accommodated by fracturing the matrix of volcanogenic and limestone conglomerates (Fig. 11c, d) and the massive bioclastic limestone (Fig. 11a), and by faulting at the contacts between different lithological units (Fig. 11b). The many planes of preexisting weaknesses in the hanging wall (i.e., weak layer boundaries) compared to the fewer planes of preexisting weaknesses in the footwall (i.e., thick and competent blocks) could explain why more strain was localized within the hanging wall.

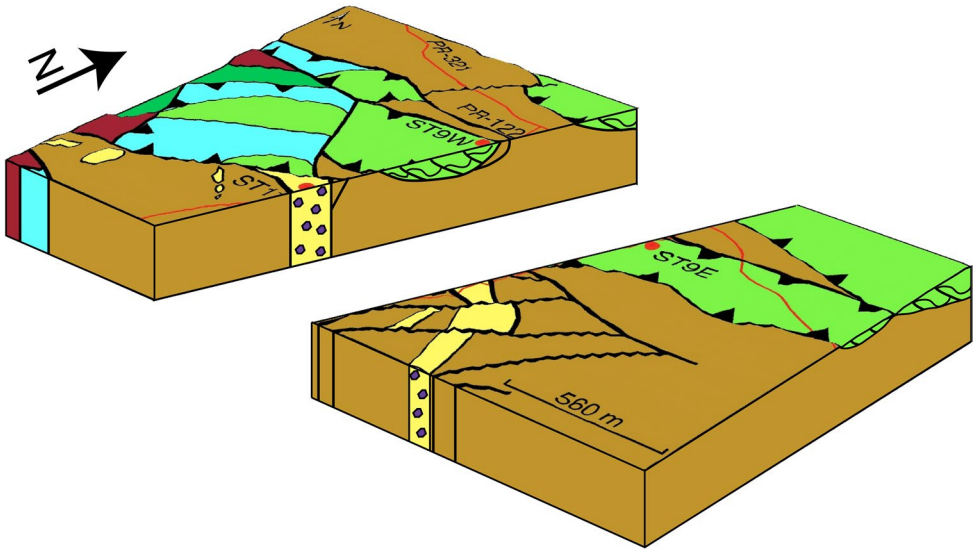

Fig. 15 3D view of the RGFT belt. Geology from Fig. 3 was draped over a Shuttle Radar Topography Mission Digital Elevation Model with vertical exaggeration of 10. Interpreted cross section shows the thrust sheet that was transported toward the SW. Imbricate thrusts may have transferred strain from the detachment to the hanging wall rocks where it was accommodated by the flexural slip mechanism. Footwall rocks also accommodated strain from the contractional event (see text for details)

Back arc deformation

The Yauco and El Rayo Formations represent sedimentary sequences that formed in environments near an island-arc. The volcanic centers in Puerto Rico during the Late Cretaceous and Eocene occur in the Central Block as indicated by the location of the Utuado Pluton and San Lorenzo Batholith (Fig. 1). The Yauco Formation formed south of this volcanic center in a basin where marine carbonate sediments and epiclastic material of volcanic origin accumulated. Larue et al. (1991) suggests that the Yauco Formation originated in an intra-arc basin in the Late Cretaceous. The El Rayo Formation formed closer to a volcanic source south of the island's volcanic center. The formation contains rocks from volcanic, epiclastic and carbonate environments. These materials were occasionally reworked and mixed in near-shore environments, and in some cases, carbonate sediment was derived from carbonate platform sources. The juxtaposition of the Yauco and El Rayo Formations that originated in different environments and the structural information analyzed in this study indicate crustal shortening (Fig. 15). The location of the subduction zone to the north of Puerto Rico since the formation of the island arc in the Early Cretaceous (Boschman et al. 2014), the location of the volcanic centers in the Central Block, and the SW vergence of the thrust system suggest that the deformation occurred in the back arc of the island arc. Thus, the Río Guanajibo fold-and-thrust belt represents the Paleogene back arc deformation of a bivergent thrust system in the northeastern Caribbean (Fig. 16).

The crustal deformation is described as a major NNE–SSW shortening event that produced folding, and reverse, thrust and left-lateral faulting in the upper crust during

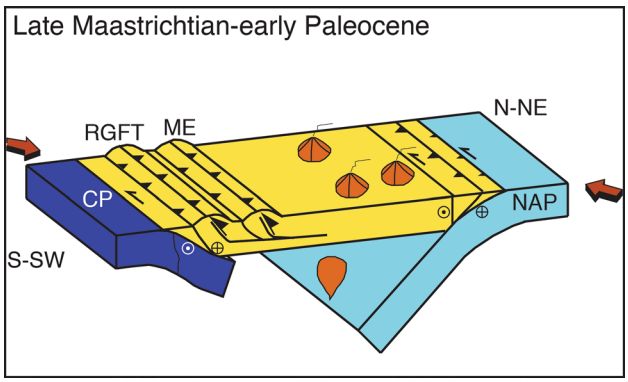

Fig. 16 Geodynamic regional model of the Puerto Rico region in the Late Maastrichtian–Paleocene (modified from Laó-Dávila et al. 2012). The RGFT and the deformation in the Monte del Estado (ME) formed in the back arc of the subduction zone of the North American Plate (NAP). The Caribbean Plate (CP) underthrust the Puerto Rico terrane. Oblique motion of contraction created transpression at the northern and southern margins

the Paleocene–Eocene. This event is correlated with the proposed collisional tectonic events in the northern margin of the Caribbean during this time, which transmitted stresses to the back arc region of Hispaniola and Puerto Rico (Laó-Dávila 2014). A later E–W shortening event was accommodated along steep structures and may have occurred by counterclockwise rotation of Puerto Rico during the Eocene (van Fossen et al. 1989; Laó-Dávila and Anderson 2009). Subsequent normal faulting was produced by extension with similar orientation to the extension described in younger Oligocene and Miocene carbonates in southern Puerto Rico and suggests that these faults formed by the same extensional event (Mann et al. 2005).

Conclusions

New road cuts along the foreland of the Río Guanajibo fold-and-thrust belt provide insights on the deformation of the hanging wall and footwall within this thrust system. We described the nature and orientation of meso-structures to characterize the folding mechanisms, kinematics, and strain accommodation within blocks of the fold-and-thrust belt. The hanging wall shows a sequence of folded, medium-bedded mudstone and thinly bedded shale and sandstone of the Yauco Formation. Fold orientations and kinematic analysis of reverse and left-lateral faults within the hanging wall suggest a strong NE–SW shortening direction that formed during pure shear strain. Right-lateral faults indicate that an E–W shortening event reactivated some of the structures. Normal faults extended the rocks most likely in the Neogene. During the major deformational event, flexural slip, reverse and strike-slip faulting, and veining accommodated the strain in the hanging wall. At the footwall, bioclastic limestone and polymictic orthoconglomerates and paraconglomerates comprise a mixture of lithological units in the El Rayo Formation. Steeply inclined reverse and strike-slip faults cut through the blocks and along lithological contacts. Kinematic analysis and descriptions of fault orientations suggest N–S shortening in a contractional regime. These results suggest that both the hanging wall and footwall accommodated strain along preexisting weaknesses, although the weaknesses are of different nature due to their different sedimentary structures and composition. The Río Guanajibo fold-and-thrust belt represents the Paleogene back arc deformation of a bivergent thrust system in the northeastern Caribbean.

Acknowledgments The Boone Pickens School of Geology provided funds for transportation to D. A. Laó-Dávila. P. A. Llerandi-Román thanks the College of Liberal Arts and Science and the Department of Geology at Grand Valley State University for granting a sabbatical leave that allowed him to collect data for this project. The authors thank Michael Martínez for helping to identify the rudist fossils, Dominike Merle Johnson for providing comments to a previous version of the manuscript, and Carlos Cuebas Matos for informing us of the existence of the outcrops. Mohamed Abdelsalam provided artwork guidance. The comments of one anonymous reviewer improved the manuscript. This is Oklahoma State University Boone Pickens School of Geology contribution number 2015-34.

References

Boschman LM, van Hinsbergen DJJ, Torsvik TH, Spakman W, Pindell JL (2014) Kinematic reconstruction of the Caribbean region since the Early Jurassic. Earth Sci Rev 138:102–136. doi:10.1016/j.earscirev.2014.08.007

Boyer SE, Elliott D (1982) Thrust systems. AAPG Bull 66:1196–1230

Curet AF (1981) The geology of a Cretaceous-Tertiary volcano-sedimentary sequence in the Mayaguez and Rosario quadrangles in west-central Puerto Rico, Ph.D. University of California, Santa Barbara

Davis D, Suppe J, Dahlen FA (1983) Mechanics of fold-and-thrust belts and accretionary wedges. J Geophys Res 88:1153–1172

Dolan J, Mann P, de Zoeten R, Heubeck C, Shiroma J, Monechi S (1991) Sedimentologic, stratigraphic, and tectonic synthesis of Eocene–Miocene sedimentary basins, Hispaniola and Puerto Rico. In: Mann P, Draper G, Lewis JF (eds) Geologic and tectonic development of the North America-Caribbean Plate Boundary in Hispaniola, vol 262. Geological Society of America, Boulder, CO, pp 217–264

Erikson JP, Pindell JL, Larue DK (1990) Mid-Eocene-early Oligocene sinistral transcurrent faulting in Puerto Rico associated with formation of the northern Caribbean plate boundary zone. J Geol 98:365–384

Fowler TJ (1996) Flexural-slip generated bedding-parallel veins from central Victoria, Australia. J Struct Geol 18:1399–1415

Glover III L (1971) Geology of the Coamo area, Puerto Rico, and its relation to the volcanic arc-trench association. US Geological Survey Professional Paper 636, p 102

Hess HH, Otalora G (1964) Mineralogical and chemical composition of the Mayaguez serpentinite cores. In: a study of serpentinite, pp 152–168

Heubeck C, Mann P (1991) Structural geology and Cenozoic tectonic history of the southeastern termination of the Cordillera Central, Dominican-Republic. In: Mann P, Draper G, Lewis JF (eds) Geologic and tectonic development of the North America-Caribbean Plate Boundary in Hispaniola, vol 262. Geological Society of America, Boulder, CO, pp 315–336

Lagabrielle Y, Pelletier B, Cabioch G (2003) Coseismic and long-term vertical displacement due to back arc shortening, central Vanuatu: Offshore and onshore data following the Mw 7.5, 26 November 1999 Ambrym earthquake. J Geophys Res 108(B11):2519. doi:10.1029/2002JB002083

Laó-Dávila DA (2014) Collisional zones in Puerto Rico and the northern Caribbean. J S Am Earth Sci 54:1–19

Laó-Dávila D, Anderson TH (2009) Kinematic analysis of serpentinite structures and the manifestation of transpression in southwestern Puerto Rico. J Struct Geol 31:1472–1489

Laó-Dávila DA, Llerandi-Román PA, Anderson TH (2012) Cretaceous–Paleogene thrust emplacement of serpentinite in southwestern Puerto Rico. Geol Soc Am Bull 124:1169–1190. doi:10.1130/B30630.1

Larue DK, Pierce P, Erickson J (1991) Cretaceous intra-Arc summit basin on Puerto Rico. In: Gillezeau KA (ed) Transactions of the Second Geological Conference of the Geological Society of Trinidad & Tobago. Geological Society of Trinidad and Tobago, pp 184–190

Lewis JF, Draper G, Fernández JAP, Espaillat J, Jiménez J (2006) Ophiolite-related ultramafic rocks (serpentinites) in the Caribbean region: a review of their occurrence, composition, origin, emplacement and Ni-laterite soil formation. Geologica Acta 4(1):237

Llerandi Román PA (2004) The Geology of the western section of the Sabana Grande quadrangle: implications for the geological evolution of southwestern Puerto Rico, M.S. University of Puerto Rico

Mann P, Draper G, Lewis JF (1991) An overview of the geologic and tectonic development of Hispaniola. In: Mann P, Draper G, Lewis JF (eds) Geologic and tectonic development of the North America-Caribbean Plate Boundary in Hispaniola, vol 262. Geological Society of America, pp 1–28

Mann P, Hippolyte J-C, Grindlay NR, Abrams LJ (2005) Neotectonics of southern Puerto Rico and its offshore margin. In: Mann P (ed) Active tectonics and seismic hazards of Puerto Rico, the Virgin Islands, and offshore areas, vol 385. Geological Society of America Special Paper. Geological Society of America, Boulder, Colorado, pp 173–214

Marrett R, Allmendinger RW (1990) Kinematic analysis of fault-slip data. J Struct Geol 12:973–986

Martínez Colón M (2003) Geologic and tectonic history of the eastern section of the Sabana Grande quadrangle, M.S. University of Puerto Rico

Mattson PH (1960) Geology of the Mayagüez area, Puerto Rico. Geol Soc Am Bull 71:319–362

Mattson PH (1964) Petrography and structure of serpentinite from Mayaguez, Puerto Rico. In: a study of serpentinite, pp 7–24

McIntyre DH, Aaron JM, Tobisch OT (1970) Cretaceous and lower Tertiary stratigraphy in northwestern Puerto Rico. U S Geological Survey Bulletin 1294-D, p 16

Mitchell SF, Martínez-Colón M, Ramsook R, Santos H (2012) A primitive tube-bearing antillocaprinid rudist bivalve, *Parasarcolites sohli* sp. nov, from Jamaica and Puerto Rico. West Indies Cretac Res 34:149–153. doi:10.1016/j.cretres.2011.10.013

Monroe WH (1980) Geology of the middle Tertiary formations of Puerto Rico. U.S. Geological Survey, Washington, D.C.

Naylor M, Sinclair HD (2008) Pro- vs. retro-foreland basins. Basin Res 20:285–303. doi:10.1111/j.1365-2117.2008.00366.x

Pessagno EAJ (1960) Geology of the Ponce-Coamo area, Puerto Rico, Ph.D. Princeton University

Pessagno EA (1962) The Upper Cretaceous stratigraphy and micropaleontology of south-central Puerto Rico. Micropaleontology 8:349–368

Plafker G, Ward SN (1992) Backarc thrust faulting and tectonic uplift along the Caribbean sea coast during the April 22, 1991 Costa Rica earthquake. Tectonics 11(4):709–718

Ryan WB et al. (2009) Global multi-resolution topography synthesis. Geochem Geophys Geosyst 10

Santos H (1999) Stratigraphy and depositional history of the upper Cretaceous strata in the Cabo Rojo-San German structural block, southwestern Puerto Rico, Ph.D. University of Colorado

Silver EA, Reed D, McCaffrey R, Joyodiwiryo Y (1983) Back arc thrusting in the Eastern Sunda Arc, Indonesia: a consequence of arc-continent collision. J Geophys Res Solid Earth (1978–2012) 88:7429–7448

Slowdowski TR (1956) Geology of the Yauco area, Puerto Rico, Ph.D. Princeton University

Snyder DB, Prasetyo H, Blundell DJ, Pigram CJ, Barber AJ, Richardson A, Tjokosaproetro S (1996) A dual doubly vergent orogen in the Banda Arc continent-arc collision zone as observed on deep seismic reflection profiles. Tectonics 15:34–53

Suárez G, Pardo M, Dominguez J, Ponce L, Montero W, Boschini I, Rojas W (1995) The Limon, Costa Rica earthquake of April 22, 1991: back arc thrusting and collisional tectonics in a subduction environment. Tectonics 14:518–530

Tanner PG (1989) The flexural-slip mechanism. J Struct Geol 11:635–655

Tanner PW (1992) Morphology and geometry of duplexes formed during flexural-slip folding. J Struct Geol 14:1173–1192

ten Brink US, Marshak S, Bruna JLG (2009) Bivergent thrust wedges surrounding oceanic island arcs: insight from observations and sandbox models of the northeastern Caribbean plate. Geol Soc Am Bull 121:1522–1536. doi:10.1130/B26512.1

van Fossen MC, Channell JET, Schellekens JH (1989) Paleomagnetic evidence for Tertiary anticlockwise rotation in southwest Puerto Rico. Geophys Res Lett 16:819–822

Volckmann RP (1984) Geologic map of the San German Quadrangle, Southwest Puerto Rico. United States Geological Survey, Washington, D.C.

Wadge G, Draper G, Lewis JF (1984) Ophiolites of the northern Caribbean: a reappraisal of their roles in the evolution of the Caribbean plate boundary. In: Gass IG, Lippard SJ, Shelton AW (eds) Ophiolites and oceanic lithosphere. Blackwell Scientific Publications, Oxford, pp 367–380

Willett S, Beaumont C, Fullsack P (1993) Mechanical model for the tectonics of doubly vergent compressional orogens. Geology 21:371–374

Witschard M, Dolan JF (1990) Contrasting structural styles in siliciclastic and carbonate lithologies of an offscraped sequence: the Peralta accretionary prism, Hispaniola. Geol Soc Am Bull 102:792–806